Science Advances
AAAS

advances.sciencemag.org/cgi/content/full/6/49/eabb8680/DC1

Supplementary Materials for

Oligodendroglial glycolytic stress triggers inflammasome activation and neuropathology in Alzheimer's disease

Xinwen Zhang, Rihua Wang, Di Hu, Xiaoyan Sun, Hisashi Fujioka, Kathleen Lundberg, Ernest R. Chan, Quanqiu Wang, Rong Xu, Margaret E. Flanagan, Andrew A. Pieper, Xin Qi*

*Corresponding author. Email: xxq38@case.edu

Published 4 December 2020, *Sci. Adv.* **6**, eabb8680 (2020)
DOI: 10.1126/sciadv.abb8680

This PDF file includes:

Supplementary methods

Computational virtual screening of HK1 in AD phenotypes and associated genes

Chemical-gene network (ChemicalGN) ChemicalGN contains 473,602 chemical nodes, 18,701 gene nodes, and 15,473,939 genes. We obtained genes associated with microbial metabolites from the STITCH (Search Tool for Interactions of Chemicals) database. This database contains 15,473,939 chemical-gene associations found in the human body, representing 473,602 chemicals and 18,701 human genes (data accessed in June 2019). Among the 220 microbial human metabolites, 216 mapped to chemicals in STITCH. For example, TMAO was associated with 293 genes, butyric acid was associated with 815 genes, and gamma-aminobutyric acid was associated with 711 genes. The human microbial metabolite-gene network consisted of 216 metabolite nodes, 11,914 gene nodes and 67,012 microbial metabolite-gene edges.

Mutational phenotype-gene network (PhenGN) PhenGN consists of 9,982 phenotype nodes, 11,021 gene nodes, and 517,381 phenotype-gene edges. We obtained a total of 517,381 systematic genetic knockouts of phenotype-gene associations (9,982 phenotypes and 11,021 mapped human genes) from the Mouse Genome Database (MGD). We previously used these strong causal gene-phenotype associations for screening functional effects of chemicals on disease phenotypes and validated our virtual screening drug candidates in experimental models of ovarian cancer. In this study, we developed network-based prediction models leveraging these causal phenotype-gene associations to assess how mutations of specific genes affected Alzheimer-related phenotypes, such as "*amyloid beta deposits,*" "*tau protein deposits,"* or "*neurodegeneration.*"

Pathway-Gene network (PathGN) PathGN contains 8,868 gene nodes, 1,329 pathway nodes, and 66,293 gene-pathway edges. We obtained a total of 66,293 canonical gene-pathway associations for 8,868 genes and 1,329 pathways from the Molecular Signatures Database (MSigDB) (data accessed in June 2019). MSigDB is currently the most comprehensive resource of annotated pathways and gene sets.

Protein-protein interaction network (PPIN) PPIN contains 22,982 gene nodes and 382,256 gene-gene edges. We obtained a total of 382,256 gene-gene associations (22,982 human genes) from BioGrid.

Prioritization algorithm

The goal of this study was to prioritize genes, pathways, and phenotypes for the input gene HK1. For the input gene, we prioritized other biomedical entities using the context-sensitive network-based ranking algorithm. The random walk-based approach is briefly described below. We regulated the movements of a random walker between any two sub-networks with jumping probabilities $\lambda_{N_iN_j}$ (N_i and N_j can be any of the four sub-networks). For example, if a random walker stands on a gene node in ChemicalGN, which was connected to PhenGN, PathGN, and PPIN, it could walk to PhenGN with the probability λ_{12}, to PathGN with the probability $\lambda_{13,}$ or to PPIN with the probability λ_{14}. It could also stay within $ChemicalGN$ with the probability $1 - \lambda_{12} - \lambda_{13} - \lambda_{14}$. Given the seed node HK1, the ranking score for each node in the network is iteratively updated by:

$$S_{k+1} = \alpha M^T S_k + (1-\alpha) S_0 , \quad (1)$$

S_{k+1} is the score vector at step k + 1, S_0 is the initial vector, $1-\alpha$ is the restarting probability, and M is the transition matrix. We calculated the transition matrix M in (2) - (3):

$$M = \begin{bmatrix} M_1 & M_{1.} & M_{1n} \\ M_{m1} & M_m & M_{mn} \\ M_{n1} & M_{n.} & M_n \end{bmatrix} \quad (2)$$

M consisted of 16 sub-matrices, each containing the transition probabilities within or between the four sub-networks. Each sub-matrix was calculated by normalizing the rows in the adjacency matrix of the corresponding sub-networks using the jumping probabilities. Specifically, the off-diagonal sub-matrices corresponded to the bipartite networks that connect every two networks. These sub-matrices were calculated by first normalizing the rows of the bipartite network $A_{N_iN_j}$, and then weighing each row by the jumping probability $\lambda_{N_iN_j}$:

$$(M_{N_iN_j})_{kl} = \begin{cases} \lambda_{N_iN_j}(A_{N_iN_j})_{kl} / \sum_l (A_{N_iN_j})_{kl} & \sum_l (A_{N_iN_j})_{kl} \neq 0 \\ 0 & otherwise \end{cases} \quad (3)$$

The diagonal submatrices corresponded to the transition probabilities within each one of the four subnetworks. They were calculated by first normalizing the rows of adjacency matrix for $ChemicalGN, PhenGN, PPIN, and\ PathGN$ and then weighing the rows by the probability of staying in the same network:

$$(M_{N_i})_{kl} = (1 - \sum I_{N_j} \lambda_{N_iN_j}) (A_{N_i})_{kl} / \sum_l (A_{N_i})_{kl} \quad (4)$$

In (4), A_{N_i} is the adjacency matrix of the submatrix N_i, and I_{N_j} is an indicator function, whose value is 1 if the *kth* row of $A_{N_iN_j}$ contains at least one non-zero element. The output from the CSN-based algorithm was a list of phenotypes, genes, pathways, and chemicals for the input gene HK1 ranked based on their genetic, functional, and phenotypic relevance to the input gene.

Evaluation of AD-associated phenotypes

There is a large, ongoing effort to characterize AD models and identify core AD-related phenotypes (https://www.alzforum.org/research-models/alzheimers-disease/commonly-used). Thirteen AD-associated phenotypes were obtained from the Research Models at Alzforum database: *amyloid beta deposits*, *amyloidosis*, *cerebral amyloid angiopathy*, *neurofibrillary tangles*, *tau protein deposits*, *neurodegeneration*, *neuron degeneration, gliosis, astrocytosis, microgliosis, abnormal synaptic transmission, abnormal long-term potentiation*, and *abnormal long-term depression*. These 13 phenotypes included a range of the core AD-related phenotypes, including plaques, tangles, neuronal loss, gliosis, synaptic loss, changes in LTP/LTD, cognitive impairment. The above network-based prioritization algorithm (input: HK1; output: a list of prioritized mouse mutational phenotypes) was evaluated using these 13 AD-related phenotypes to examine how HK1 is phenotypically related to AD.

Evaluation of AD-associated genes

In this study, we used 22 genes that were strongly associated with or causally involved in AD from the Online Mendelian Inheritance in Man (OMIM) database, a knowledgebase of human genes and genetic disorders, and ClinVar: public archive of interpretations of clinically relevant variants. These 22 strong AD genes were *A2M, ABCA7, ACE, ADAM10, APBB2, APOE, APP, BLMH, HFE, MPO, MT-ND1, NOS3, PAXIP1, PLAU, PLD3, PRNP, PSEN1, PSEN2, SORL1, TF, TNF*, and *VEGFA*. The network-based prioritization algorithm (input: HK1;

output: a list of prioritized human genes) was evaluated using these 22 AD genes to examine how HK1 is genetically related to AD.

Supplementary Figure legends

Figure S1: NLRP3 inflammasome activation and GSDMD-mediated pyroptotic injury in mature OLs of AD mice. The brains of WT and 5XFAD mice were harvested at the ages of 3, 6, and 9 months (n = 3−4 mice/group). (A) Brain sections were stained with anti-NLRP3 and anti-CC1 antibodies. Scale bar is 20 μm. (B) The intensity of NLRP3 in the $CC1^+$ OLs was quantified. Brain sections were also stained with anti-Iba1 and anti-GFAP antibodies. The intensities of Iba1 and GFAP in the corpus callosum were quantified and presented in (C) and (D). Data are expressed as the mean ± SEM and compared by one-way ANOVA with Tukey's *post-hoc* test. (E) The brain sections of 6-month-old WT and 5XFAD mice were stained with anti-GSDMD and anti-GFAP antibodies. GSDMD positive signal was rarely observed in $GFAP^+$ astrocytes in the 5XFAD mice. Scale bar is 20 μm. (F) The brain sections of 6-month-old WT and 5XFAD mice were stained with anti-GSDMD and anti-Iba1 antibodies or anti-NLRP3 and anti-Iba1 antibodies. Scale bar is 20 μm. (G) Total protein lysates were isolated from the corpus callosum of WT and 5XFAD mice (n = 3 mice/group) at ages of 3 and 6 months. Western blot analysis was performed with the indicated antibodies. The densities of NLRP3, cleaved caspase-1, GSDMD (CL), and mature IL-1β relative to actin are shown in the histograms. Data are expressed as the mean ± SEM. Student's *t*-test. (H) The brain sections of mice were stained with anti-MBP or the Black Gold II myelin staining kit. Scale bar is 200 μm. (I) The MBP-positive area was measured. The data were compared by one-way ANOVA with Tukey's *post-hoc* test. (J) The brain sections of 6-month-old WT and 5XFAD mice (n=3 mice/group) were stained with anti-GSDMD, anti-Iba1, and anti-6E10 antibodies.

Figure S2: Changes of NLRP3 inflammasome and mitochondrial dynamics related proteins in mature OLs and in 5XFAD mice. Mature OLs were differentiated from OPCs and exposed to oligomeric $A\beta_{1\text{-}42}$ (5 μM) at the indicated periods. NLRP3 protein levels (A) and the cleavage of GSDMD (B) were examined by western blot analysis. Histogram: the relative density of NLRP3 and GSDMD cleavage versus actin. (C) The medium was collected from mature OLs exposed to oligomeric $A\beta_{1\text{-}42}$ at the indicated time points. The released IL-1β in the medium was measured by ELISA. 3 independent experiments were carried out. (D) Mature OLs were differentiated from OPCs and exposed to oligomeric $A\beta_{42\text{-}1}$ (5 μM) at the indicated periods. Western blot analysis was performed with the indicated antibodies. Histogram: the relative density of NLRP3 and GSDMD cleavage versus actin. (E) The medium was collected from mature OLs exposed to oligomeric $A\beta_{42\text{-}1}$ at the indicated time points. Released IL-1β was measured by ELISA. (F) The release of LDH was analyzed in mature OLs exposed to oligomeric $A\beta_{1\text{-}42}$ at the indicated concentrations. (G) Total protein lysates isolated from the corpus callosum of WT and 5XFAD mice were obtained at ages of 3 and 6 months (n = 3-4 mice/group). Western blot analysis was carried out with the indicated antibodies. Data are expressed as the mean ± SEM. Student's *t*-test. Mature OLs were differentiated from OPCs and exposed to oligomeric $A\beta_{42\text{-}1}$ (5 μM) at the indicated periods. (H) Drp1 oligomerization was measured in the presence or absence of β-ME. (I) Western blot analysis was carried out with the indicated antibodies. At least 3 independent experiments were performed in the cultured cells. All data in cell culture are expressed as the mean ± SEM and compared by one-way ANOVA with Tukey's *post-hoc* test.

Figure S3: Suppression of Drp1 hyperactivation in mature OLs. Mature OLs were differentiated from OPCs. (A) Cells were infected with lentivirus encoding Drp1 or control shRNA for 48 hours and maintained in the cell culture medium with puromycin (1μg/mL). The Drp1 knockdown efficiency was validated by western blot analysis. (B) After exposure to oligomeric $A\beta_{1\text{-}42}$ (5 μM, 24 hours), Drp1 ser616 phosphorylation was determined by western blot analysis and the density of Drp1 ser616 phosphorylation relative to actin is shown in the histogram. Mature OLs were treated with Mdivi-1 (5 μM) for 4 hours before treatment with oligomeric $A\beta_{1\text{-}42}$ (5 μM) for 24 hours. Drp1 ser616 phosphorylation (C) and Drp1 tetramer (D) levels were determined by western blot analysis. The relative densities of Drp1 ser616 phosphorylation and Drp1 tetramer are shown in the histogram. (E) Western blot analysis of total protein lysates harvested from mature OLs of the indicated groups was performed with the indicated antibodies. The quantification of these protein changes is shown in the histogram. (F) The release of IL-

1β into the medium of the indicated groups was analyzed by ELISA. Data are expressed as the mean ± SEM from at least 3 independent experiments and compared by One-way ANOVA with Tukey's *post-hoc* test.

Figure S4: The effects of mature OL Drp1 heterozygous knockout in 5XFAD mice. (A) The illustration of the generation of mature OL Drp1 heterozygous knockout 5XFAD mice. (B) Body weight of mice with the indicated genotypes was recorded with age. 8 female and 7 male WT, 8 female and 8 male CNP;$Drp1^{fl/+}$, 8 female and 8 male $5XFAD^{het}$;$Drp1^{+/+}$, 7 female and 7 male $5XFAD^{het}$;CNP;$Drp1^{fl/+}$ mice were used. (C) Brain sections of 6-month-old mice with the indicated genotypes were stained with anti-Drp1 and anti-CC1 antibodies. Scale bar is 20 μm. The immunodensity of Drp1 in the $CC1^+$ OLs was quantified. (D) Brain sections of six-month-old mice with the indicated genotypes were stained with anti-Drp1 and anti-GFAP or anti-NeuN antibodies. Scale bar is 20 μm. The intensity of Drp1 in the $NeuN^+$ neurons was quantified. (E) Brain sections of mice were stained with anti-neurofilament (NF) and anti-MBP antibodies. The intensity of MBP (F) and NF (G) in the corpus callosum was quantified and shown in the histogram. Brain sections of the mice with the indicated genotypes were stained with anti-GFAP or anti-Iba1 antibody. Scale bar is 50 μm. The intensity of Iba1 (H) and GFAP (I) in the corpus callosum was quantified. (J) Brain sections of mice with the indicated genotypes (n=3−4 mice/group) were stained with anti-PSD95 and anti-synaptophysin. The numbers of $PSD95^+$, $synaptophysin^+$, and colocalized presynaptic and postsynaptic puncta were counted and quantified (K, L). Data are presented as the mean ± SEM and compared by One-way ANOVA with Tukey's *post-hoc* test.

Figure S5: Proteomic analysis of mature OLs-specific Drp1 heterozygous knockout AD mice and computational analysis of HK1 with AD phenotypes and genotypes. (A) Label-free proteomic analysis of mice with the indicated genotypes identified 1098 proteins that were subjected to further analysis. (B) Bioinformatics analysis highlights the enrichment of proteins belonging to the generation of precursor metabolites and energy pathway. The heat map analysis of these proteins is shown. Among these proteins, proteins involved in glycolysis (marked in blue) were highly regulated by mature OLs-specific Drp1 heterozygous knockout. (C) Mature OLs were treated with oligomeric $A\beta_{1\text{-}42}$ for 24 hours in the presence or absence of Mdivi-1 (5 μM). The OCR were analyzed by the seahorse analyzer. The data were from 4 independent experiments. Data are expressed as the mean ± SEM and compared by one-way ANOVA with Tukey's *post-hoc* test. (D) Total protein lysates were harvested from the corpus callosum of 6-month-old mice at the indicated genotypes. Western blot analysis was performed using the anti-HK1 antibody. Actin was used as a loading control. The data were compared by one-way ANOVA with Tukey's *post-hoc* test. Computational analysis was performed to determine the implication of HK1 in AD. The method was described in the Supplementary Method section. (E) The integrated gene-pathway-phenotype network with labeled data resources was used for the computational analysis of the implication of HK1 in AD. (F) AD-specific phenotypes ranked highly for HK1. Four out of the 13 AD-associated phenotypes ranked within the top 10% (first decile) of 10,072 prioritized phenotypes. For example, phenotype "abnormal synaptic transmission" and "neurodegeneration" ranked at the top 1.92% and 8.78%, respectively. On average, AD-specific phenotypes ranked at 27.75%, which is significantly higher than random ranking (p-value = 0.006). These results indicate that HK1 is related to AD at the phenotypic level. (G) AD-specific genes ranked highly for HK1. 12 out of the 22 AD-associated genes ranked within the top 10% (first decile) among a total of 23,499 prioritized genes. For example, gene "BLMH", "VEGFA", "APP" and MT-ND1 ranked at top 0.36%, 0.39%, 0.75% and 0.78% respectively. On average, AD genes ranked at top 22.60%, which is significantly higher than random ranking (*p* value = 5.13E-5). These results indicate that HK1 is related to AD at the genetic level. (H) The top 10 ranked pathways for the input HK1 are shown. These pathways were associated with cell metabolism and immune response regulation.

Figure S6: Changes in HK1 in mature OLs of AD models *in vitro* and *in vivo*. (A) Brain sections of 6-month-old mice with the indicated genotypes were stained with anti-HK1 and anti-CC1 antibodies. The localization of HK1 in the $CC1^+$ OLs in the adjacent gray matter of mice was imaged. Scale bar is 20 μm. (B) Brain sections of 6-month-old mice with the indicated genotypes were stained with anti-CC1 and anti-HK2 antibodies. The localization of HK2 in the $CC1^+$ OLs in the corpus callosum of mice was imaged. Scale bar is 20 μm. (C) Brain sections of 6-month-old mice with the indicated genotypes were stained with anti-GFAP and anti-HK1 antibodies. The localization of HK1 in $GFAP^+$ astrocytes in the corpus callosum of mice was imaged. Scale bar is 20 μm. (D) Mitochondrial fractions and total lysates from 6-month-old mice with the indicated genotypes were isolated, and

western blot analysis was carried out with the indicated antibodies. The purity of the cellular fractionation was examined with the protein markers. ATPB: a mitochondrial inner membrane protein. Enolase: a cytosolic protein. Synaptophysin: a marker of presynapse. Tau: a marker of axons. MBP: a marker of mature OLs. (E) WT and 5XFAD mouse corpus callosum were harvested at the indicated ages. Mitochondrial and cytosolic fractions were isolated and subjected for western blot analysis. The relative densities of HK1 versus ATPB, HK1 versus enolase, Drp1 versus ATPB, and Drp1 versus enolase are shown in the histograms (n = 3 mice/group). The data were compared by Student's *t*-test. (F) Total lysates from mouse corpus callosum were immunoprecipitated with anti-VDAC antibodies. Western blot analysis was carried out with the indicated antibodies (n = 4 mice/group). Mature OLs were treated with 2-DG at the indicated concentrations for 24 hours. (G) The content of the cellular lactate was analyzed. (H) The NLRP3 protein levels were examined by western blot analysis. The relative density of NLRP3 versus actin is shown in the histogram. These data demonstrate that 2-DG-induced glycolytic inhibition induced an increase in NLRP3 protein levels in mature OLs. (I) Mature OLs were transfected with GFP-HK1 or GFP-control plasmids followed by the addition of oligomeric $A\beta_{1-42}$ (5 μM). After 24h, cells were fixed and stained with anti-Tom20 and anti-MOG antibodies. Top: representative images from three independent experiments. bottom: quantification of percentage of MOG^{+} cells with fragmented mitochondria. Scale bar: 20 μm. (J) Mature OLs were differentiated from OPCs and transfected with GFP-tagged HK1 plasmid for 48 h. Mature OLs were treated with Mdivi-1 (5 μM) 4 h before the addition of oligomeric $A\beta_{1-42}$ (5 μM) for 24 h. The protein level of NLRP3 was analyzed by western blot analysis. The density of NLRP3 relative to actin is shown in the histogram. (K) The release of IL-1β was analyzed by ELISA. All the data are expressed as the mean ± SEM, and compared by one-way ANOVA with Tukey's *post-hoc* test.

Figure S1

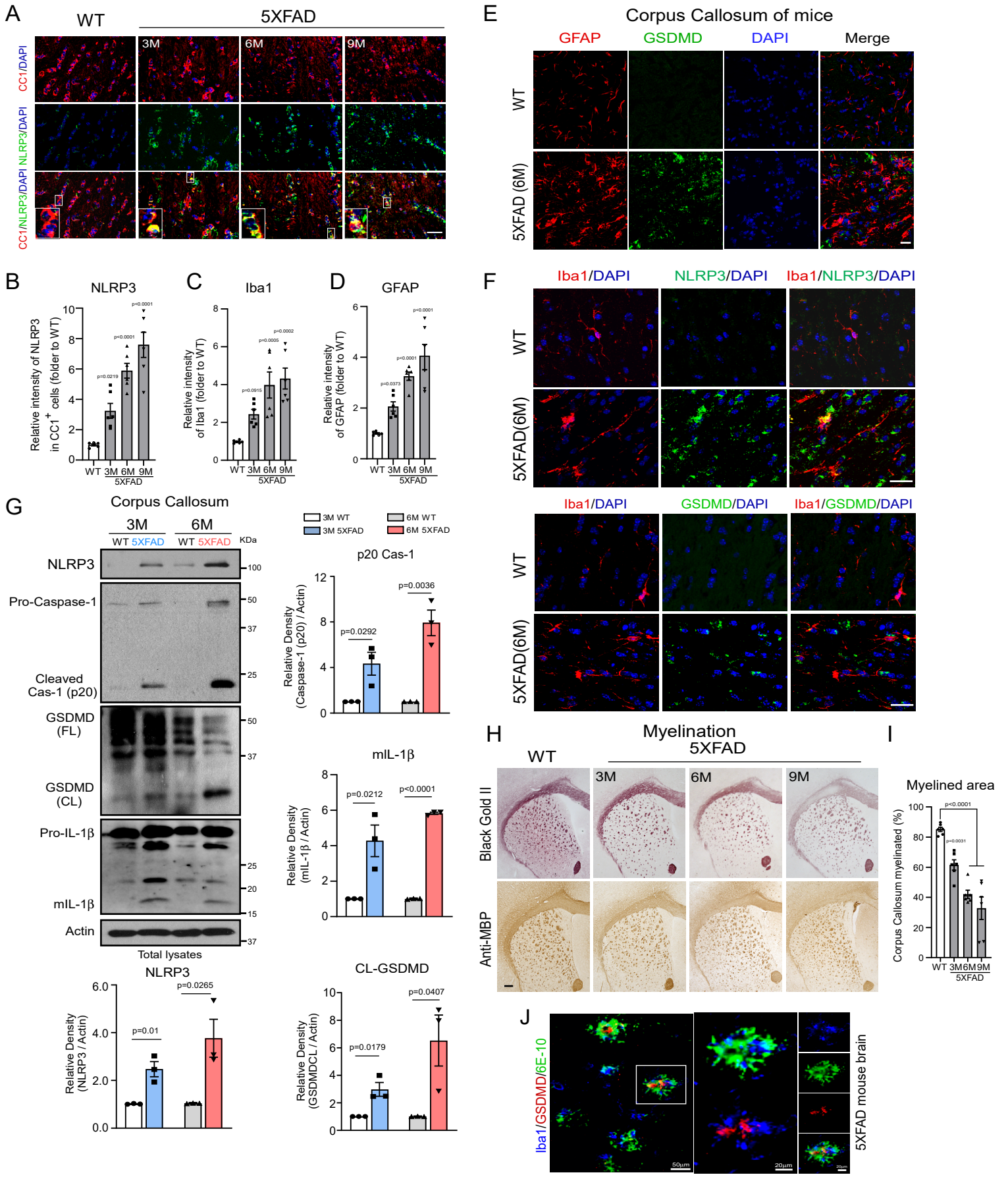
A
WT
5XFAD
3M
6M
9M
CC1/DAPI
NLRP3/DAPI
CC1/NLRP3/DAPI
B
NLRP3
Relative intensity of NLRP3 in CC1+ cells (folder to WT)
C
Iba1
Relative intensity of Iba1 (folder to WT)
D
GFAP
Relative intensity of GFAP (folder to WT)
E
Corpus Callosum of mice
GFAP
GSDMD
DAPI
Merge
WT
5XFAD (6M)
F
Iba1/DAPI
NLRP3/DAPI
Iba1/NLRP3/DAPI
Iba1/GSDMD/DAPI
5XFAD(6M)
G
Corpus Callosum
3M WT
3M 5XFAD
6M WT
6M 5XFAD
KDa
NLRP3
Pro-Caspase-1
Cleaved Cas-1 (p20)
GSDMD (FL)
GSDMD (CL)
Pro-IL-1β
mIL-1β
Actin
Total lysates
p20 Cas-1
Relative Density (Caspase-1 (p20) / Actin)
mIL-1β
Relative Density (mIL-1β / Actin)
CL-GSDMD
Relative Density (GSDMDCL / Actin)
H
Myelination
Black Gold II
Anti-MBP
I
Myelined area
Corpus Callosum myelinated (%)
J
Iba1/GSDMD/6E-10
5XFAD mouse brain

Figure S2

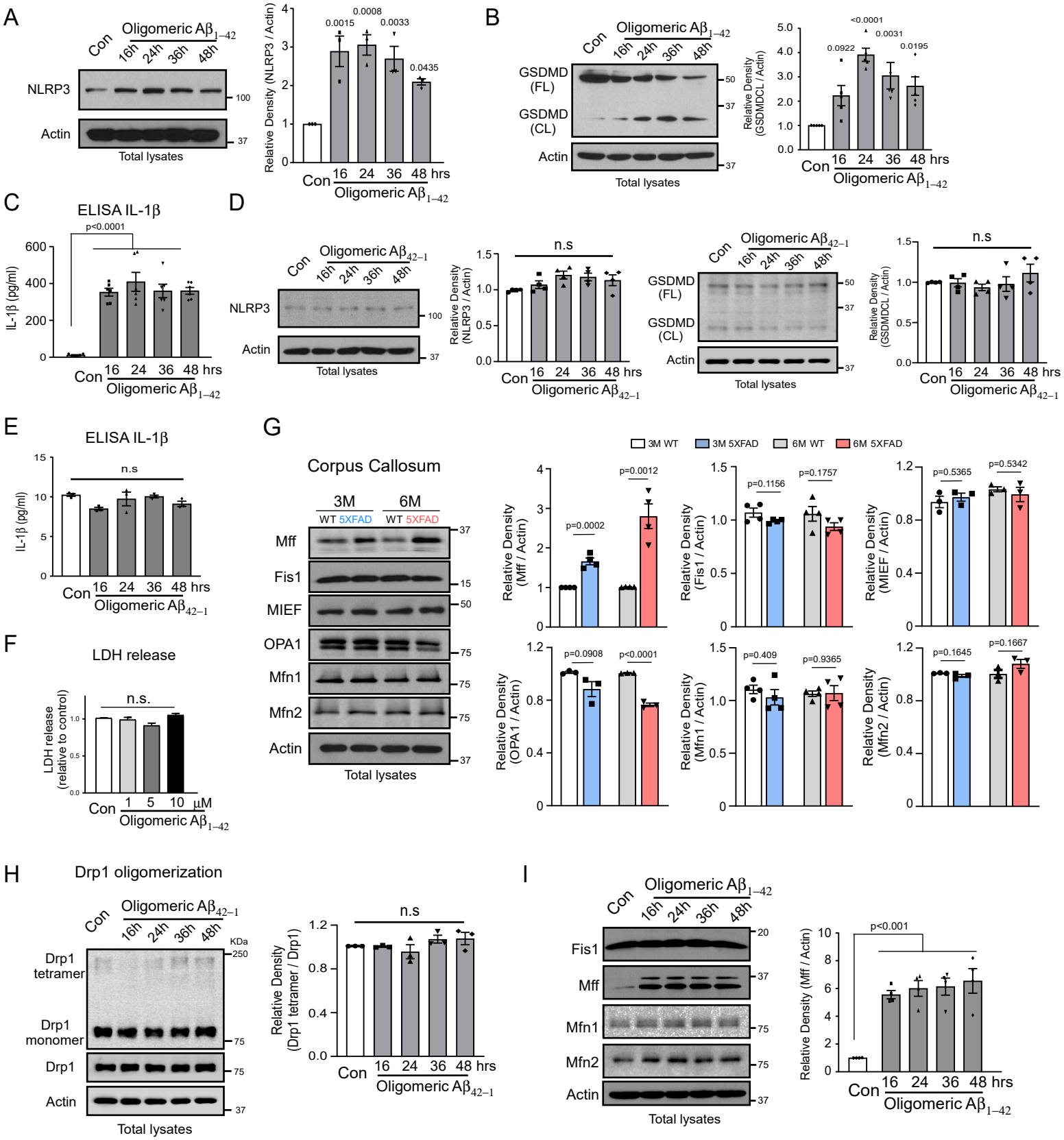
A
Oligomeric Aβ1–42
Con
16h
24h
36h
48h
NLRP3
Actin
Total lysates
Relative Density (NLRP3 / Actin)
0.0008
0.0015
0.0033
0.0435
Con 16 24 36 48 hrs
Oligomeric Aβ1–42
B
GSDMD (FL)
GSDMD (CL)
Relative Density (GSDMDCL / Actin)
<0.0001
0.0031
0.0922
0.0195
C
ELISA IL-1β
p<0.0001
IL-1β (pg/ml)
D
Oligomeric Aβ42–1
n.s
E
ELISA IL-1β
F
LDH release
n.s.
LDH release (relative to control)
Con 1 5 10 μM
G
Corpus Callosum
3M
6M
WT 5XFAD
Mff
Fis1
MIEF
OPA1
Mfn1
Mfn2
3M WT
3M 5XFAD
6M WT
6M 5XFAD
p=0.0002
p=0.0012
p=0.1156
p=0.1757
p=0.5365
p=0.5342
p=0.0908
p<0.0001
p=0.409
p=0.9365
p=0.1645
p=0.1667
H
Drp1 oligomerization
KDa
Drp1 tetramer
Drp1 monomer
Drp1
Relative Density (Drp1 tetramer / Drp1)
I
Fis1
Mff
Mfn1
Mfn2
p<0.001
Relative Density (Mff / Actin)

Figure S3

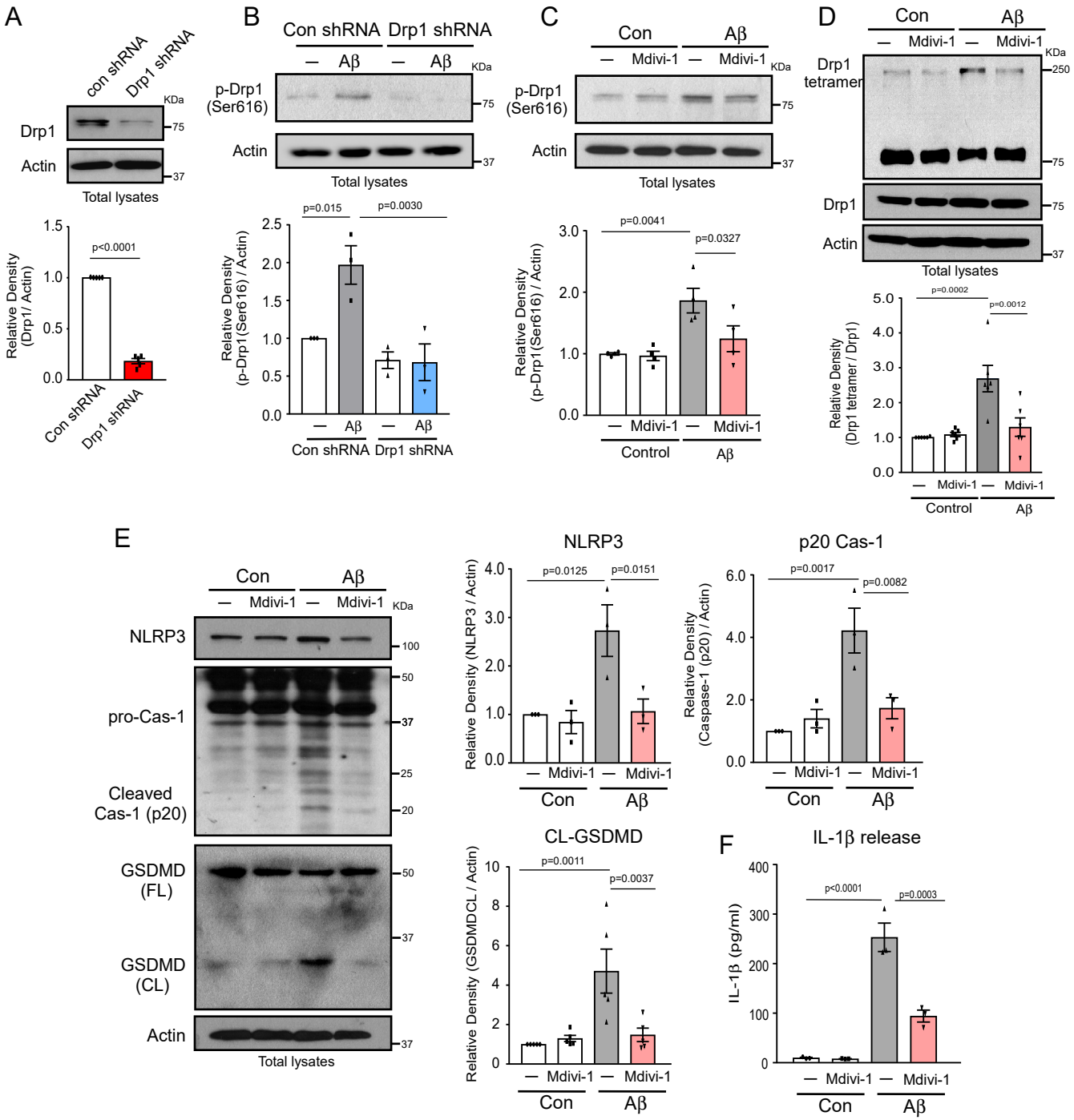
A
con shRNA
Drp1 shRNA
KDa
Drp1
75
Actin
37
Total lysates
Relative Density (Drp1/ Actin)
p<0.0001
Con shRNA
Drp1 shRNA
B
Con shRNA
Drp1 shRNA
— Aβ — Aβ
p-Drp1 (Ser616)
Actin
Total lysates
Relative Density (p-Drp1(Ser616) / Actin)
p=0.015
p=0.0030
C
Con
Aβ
— Mdivi-1 — Mdivi-1
p-Drp1 (Ser616)
Actin
Total lysates
Relative Density (p-Drp1(Ser616) / Actin)
p=0.0041
p=0.0327
Control
Aβ
D
Con
Aβ
— Mdivi-1 — Mdivi-1
Drp1 tetramer
250
Drp1
Actin
Total lysates
Relative Density (Drp1 tetramer / Drp1)
p=0.0002
p=0.0012
E
NLRP3
pro-Cas-1
Cleaved Cas-1 (p20)
GSDMD (FL)
GSDMD (CL)
Actin
100
50
37
25
20
Relative Density (NLRP3 / Actin)
p=0.0125
p=0.0151
Relative Density (Caspase-1 (p20) / Actin)
p=0.0017
p=0.0082
CL-GSDMD
Relative Density (GSDMDCL / Actin)
p=0.0011
p=0.0037
F
IL-1β release
IL-1β (pg/ml)
p<0.0001
p=0.0003

Figure S4

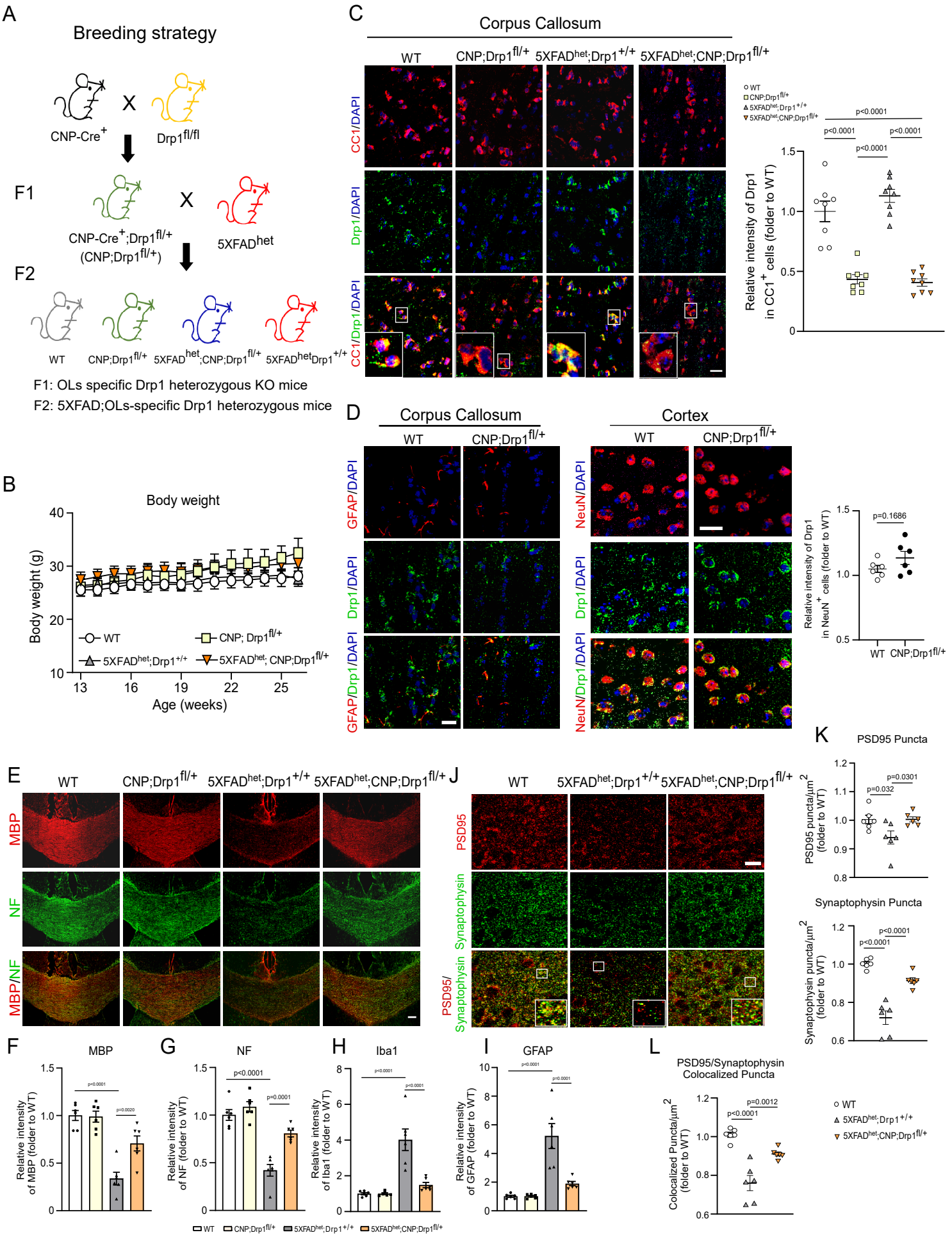
A
Breeding strategy
CNP-Cre+
X
Drp1fl/fl
F1
CNP-Cre+;Drp1fl/+
(CNP;Drp1fl/+)
X
5XFADhet
F2
WT
CNP;Drp1fl/+
5XFADhet;CNP;Drp1fl/+
5XFADhetDrp1+/+
F1: OLs specific Drp1 heterozygous KO mice
F2: 5XFAD;OLs-specific Drp1 heterozygous mice
B
Body weight
Body weight (g)
Age (weeks)
WT
CNP; Drp1fl/+
5XFADhet;Drp1+/+
5XFADhet; CNP;Drp1fl/+
C
Corpus Callosum
WT
CNP;Drp1fl/+
5XFADhet;Drp1+/+
5XFADhet;CNP;Drp1fl/+
CC1/DAPI
Drp1/DAPI
CC1/Drp1/DAPI
Relative intensity of Drp1 in CC1+ cells (folder to WT)
p<0.0001
p<0.0001
p<0.0001
p<0.0001
D
Corpus Callosum
Cortex
WT
CNP;Drp1fl/+
GFAP/DAPI
NeuN/DAPI
Drp1/DAPI
GFAP/Drp1/DAPI
NeuN/Drp1/DAPI
Relative intensity of Drp1 in NeuN+ cells (folder to WT)
p=0.1686
E
WT
CNP;Drp1fl/+
5XFADhet;Drp1+/+
5XFADhet;CNP;Drp1fl/+
MBP
NF
MBP/NF
J
WT
5XFADhet;Drp1+/+
5XFADhet;CNP;Drp1fl/+
PSD95
Synaptophysin
PSD95/Synaptophysin
K
PSD95 Puncta
PSD95 puncta/μm2 (folder to WT)
p=0.0301
p=0.032
Synaptophysin Puncta
Synaptophysin puncta/μm2 (folder to WT)
p<0.0001
p<0.0001
F
MBP
Relative intensity of MBP (folder to WT)
p<0.0001
p=0.0020
G
NF
Relative intensity of NF (folder to WT)
p<0.0001
p=0.0001
H
Iba1
Relative intensity of Iba1 (folder to WT)
p<0.0001
p<0.0001
I
GFAP
Relative intensity of GFAP (folder to WT)
p<0.0001
p<0.0001
L
PSD95/Synaptophysin Colocalized Puncta
Colocalized Puncta/μm2 (folder to WT)
p=0.0012
p<0.0001
WT
CNP;Drp1fl/+
5XFADhet;Drp1+/+
5XFADhet;CNP;Drp1fl/+

Figure S5

A

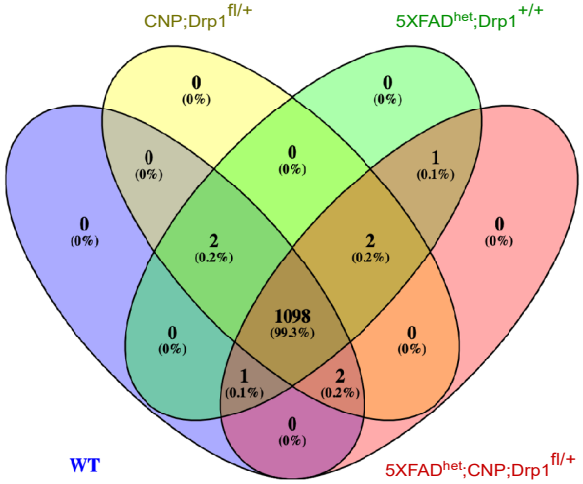

B

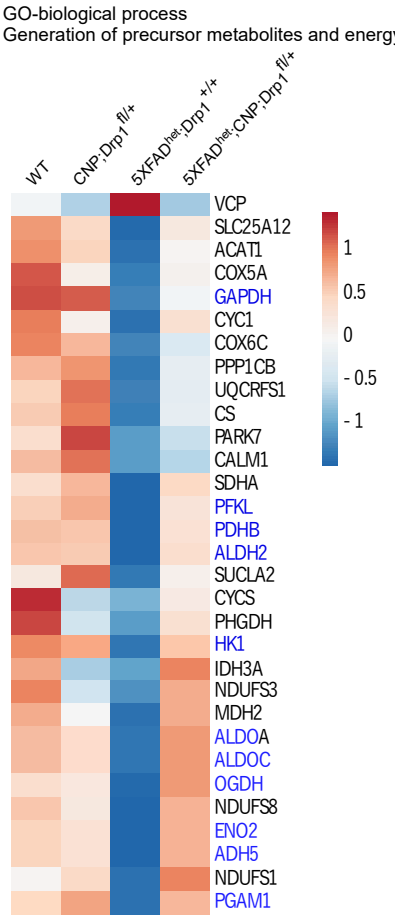

C

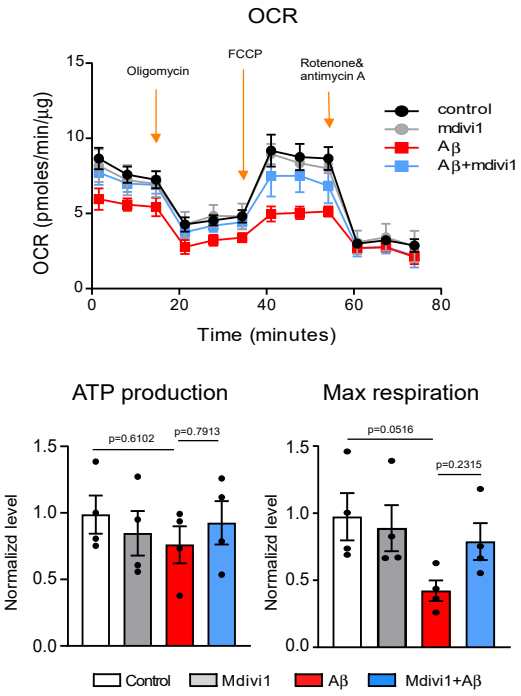

D

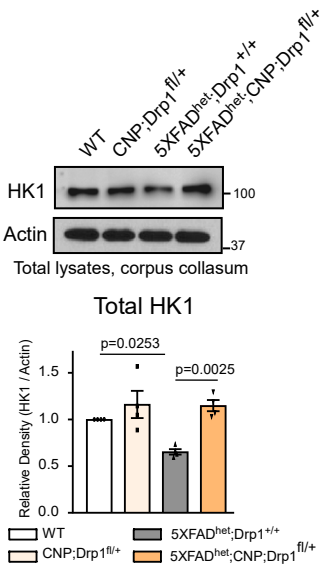

E

Numbers of sub-network nodes and edges

Subnetwork	Nodes	Nodes	Edges
Chemical-gene network	473,602 chemicals	18,701 genes	15,473,939
Mouse Phenotype-gene network	9,982 phenotypes	11,021 genes	517,381
Gene-gene interaction network	22,982 genes	22,982 genes	382,256
Gene-pathway network	8,868 genes	1329 pathways	66,293

F

Decile ranking of 13 AD-associated phenotypes among a total of 10072 prioritized phenotypes

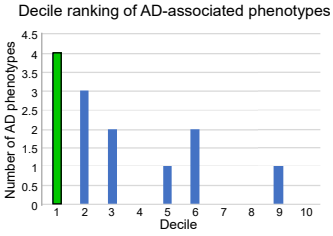

AD Phenotype	Rank (top%)	AD Phenotype	Rank (top%)
abnormal synaptic transmission	1.92	amyloid beta deposits	26.21
abnormal long term depression	4.36	amyloidosis	26.22
neurodegeneration	8.78	microgliosis	46.95
neuron degeneration	9.07	neurofibrillary tangles	54.34
gliosis	11.28	tau protein deposits	55.32
astrocytosis	16.60	cerebral amyloid angiopathy	80.20
abnormal long term potentiation	19.53		

G

Decile ranking of 22 AD-associated genes among a total of 23,499 prioritized genes

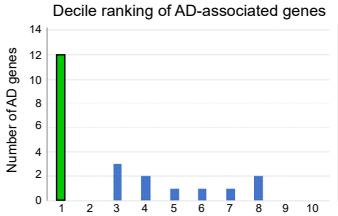

AD Gene	Rank (top%)	AD Gene	Rank (top%)
BLMH	0.36	PSEN1	9.25
VEGFA	0.39	ABCA7	23.92
APP	0.75	A2M	27.72
MT-ND1	0.78	PSEN2	29.96
NOS3	1.53	ADAM10	30.11
ACE	1.90	PLD3	37.07
APOE	2.82	PAXIP1	40.69
TF	2.94	PRNP	54.46
TNF	5.64	APBB2	64.52
PLAU	5.87	SORL1	70.63
MPO	7.06	HFE	78.96

H

Top 10 ranked pathways for the input HK1 are shown in table

Rank	Pathway
1	PPAR signaling pathway
2	GPCR signaling
3	Immune System
4	Adaptive Immune System
5	Class I MHC mediated antigen processing & presentation
6	Antigen processing: Ubiquitination & Proteasome degradation
7	Jak-STAT signaling pathway
8	IL4-mediated signaling events
9	TCR signaling in naïve CD4+ T cells
10	Metabolism of proteins

Figure S6

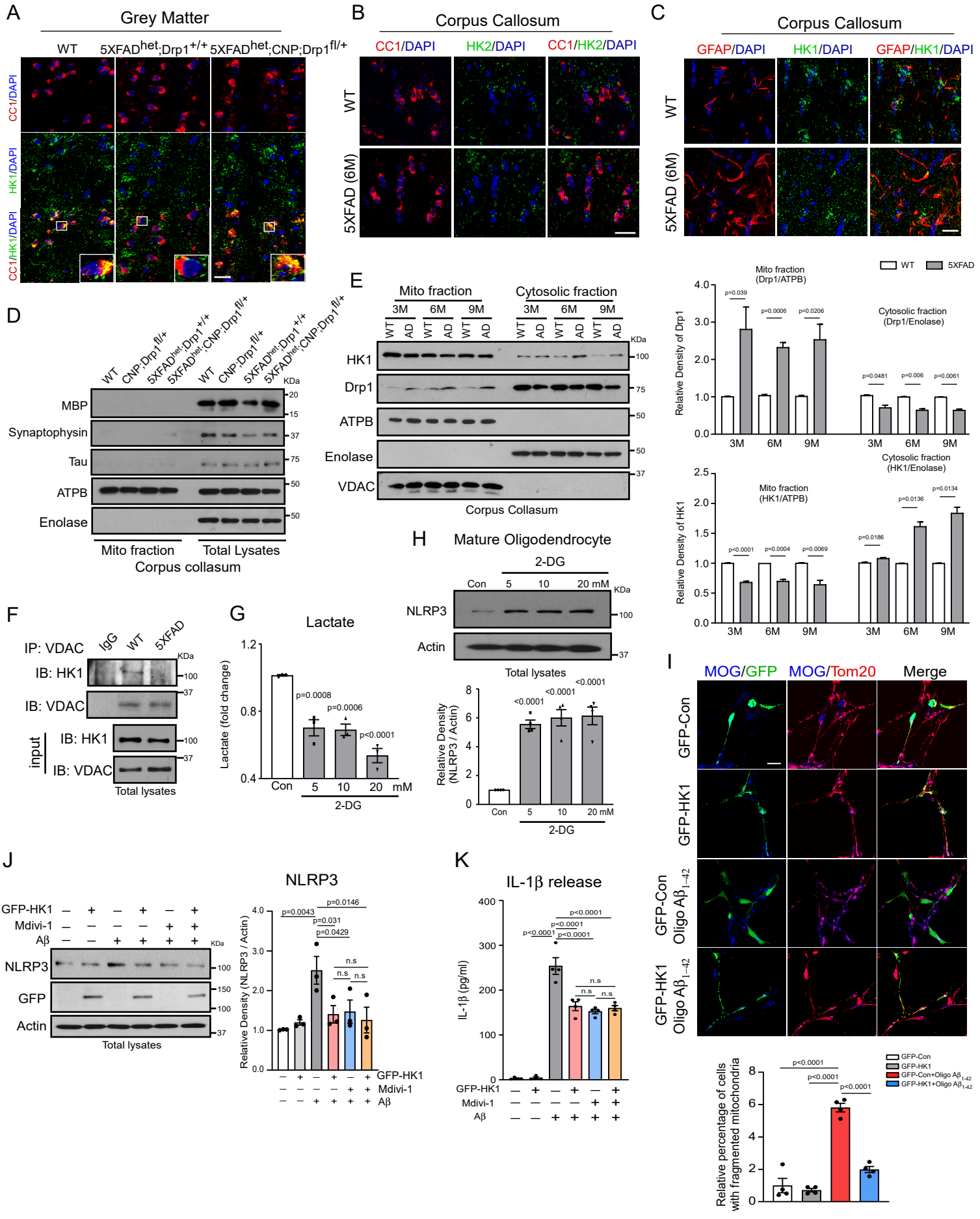
A
Grey Matter
WT
5XFAD het;Drp1 +/+
5XFAD het;CNP;Drp1 fl/+
CC1/DAPI
HK1/DAPI
CC1/HK1/DAPI
B
Corpus Callosum
CC1/DAPI
HK2/DAPI
CC1/HK2/DAPI
WT
5XFAD (6M)
C
Corpus Callosum
GFAP/DAPI
HK1/DAPI
GFAP/HK1/DAPI
WT
5XFAD (6M)
D
WT
CNP:Drp1 fl/+
5XFAD het;Drp1 +/+
5XFAD het;CNP:Drp1 fl/+
KDa
MBP
Synaptophysin
Tau
ATPB
Enolase
Mito fraction
Total Lysates
Corpus collasum
E
Mito fraction
Cytosolic fraction
3M
6M
9M
WT
AD
HK1
Drp1
ATPB
Enolase
VDAC
KDa
Corpus Collasum
WT
5XFAD
Mito fraction (Drp1/ATPB)
Relative Density of Drp1
Cytosolic fraction (Drp1/Enolase)
Mito fraction (HK1/ATPB)
Relative Density of HK1
Cytosolic fraction (HK1/Enolase)
F
IP: VDAC
IgG
WT
5XFAD
IB: HK1
IB: VDAC
input
Total lysates
G
Lactate
Lactate (fold change)
Con
5
10
20 mM
2-DG
H
Mature Oligodendrocyte
2-DG
Con
5
10
20 mM
NLRP3
Actin
Total lysates
Relative Density (NLRP3 / Actin)
I
MOG/GFP
MOG/Tom20
Merge
GFP-Con
GFP-HK1
GFP-Con Oligo Aβ1–42
GFP-HK1 Oligo Aβ1–42
Relative percentage of cells with fragmented mitochondria
J
NLRP3
GFP-HK1
Mdivi-1
Aβ
GFP
Actin
Total lysates
Relative Density (NLRP3 / Actin)
K
IL-1β release
IL-1β (pg/ml)